PERGAMON

Carbon 40 (2002) 1231–1239

CARBON

Structural and surface property changes of macadamia nut-shell char upon activation and high temperature treatment

Zheng-Ming Wang[a,*], Hirofumi Kanoh[b], Katsumi Kaneko[b], G.Q. Lu[c], Duong Do[c]

[a]*Aquamaterial Separation Technology RG, Marine Resources and Environment Institute, National Institute of Advanced Industrial Science and Technology, Hayashi-cho 2217-14, Takamatsu, Kagawa 761-0395, Japan*

[b]*Department of Chemistry, Faculty of Science, Chiba University, Yayoi 1-33, Inage-ku, Chiba 263, Japan*

[c]*Department of Chemical Engineering, University of Queensland, Brisbane, Qld 4072, Australia*

Received 19 January 2001; accepted 9 October 2001

Abstract

Structural and surface property changes of macadamia nut-shell (MNS) char upon activation and high temperature treatment (HTT) were studied by high-resolution nitrogen adsorption, diffuse reflectance infra-red Fourier transform spectroscopy, X-ray photoelectron spectroscopy, and temperature-programmed desorption. It is found that activation of MNS char can be divided into the low extent activation which may involve the reactions of internal oxygen-containing groups and leads to the formation of comparatively uniform micropores, and the high extent activation which induces reactions between carbon and activating gas and produces a large amount of micropores. The surface functional groups (SFGs) basically increase with the increase of activation extent, but high extent activation preferentially increases the amount of –C–O and –C=O. HTT in air for a short time at a high temperature (1173 K) greatly increases the micropore volume and the amounts of SFGs. By appropriately choosing the activation and HTT conditions, it is possible to control both the textural structure and the type and amounts of SFG. © 2002 Published by Elsevier Science Ltd.

Keywords: A. Activated carbon; B. Activation, Heat treatment; D. Functional groups, Microporosity

1. Introduction

Activated carbons (ACs) are porous materials with very high surface areas and large pore volumes, and have been widely used as adsorbents, separation substrates, and catalysts or catalyst supports [1,2]. The existence of large amounts of micropores provides ACs with an enhanced adsorption capacity for both the gas and liquid phases by the micropore filling mechanism [3–8]. Not only the textural structure but also the surface chemistry of carbon plays an important role in the application of ACs [9]. The hydrophobic surface of ACs leads to not only a great adsorptivity for organic vapors but also an excellent catalytic and adsorptive performance in the presence of water. The presence of surface functional groups (SFGs) on ACs allows an intense effect on their catalytic behaviors and gives the unique active sites for supporting catalytically active species [2,10–12]. Thus, in addition to great concerns about textural structures, the understanding and creation of SFGs on ACs has been the constant desire and goal for carbon scientists and engineers.

ACs are generally prepared by carbonization and physical or chemical activation of various precursors such as nut-shells, coal pitches, polymers, etc. Although the current techniques have already allowed the preparation of ACs with surface areas higher than 3000 m^2/g [13], there have been more recent efforts to find low-cost and high-yield production methods for ACs [14,15]. A theoretical calculation predicts the uppermost surface area of ACs to be 5000–6000 m^2/g for a single graphene sheet-wall model [16]. A recent improvement in fundamental adsorption theories and surface analytical tools allows a better understanding of the structural and surface properties of ACs [1,3,17,18]. During preparation of ACs, activation of a carbon precursor brings about not only pore opening but also changes in the types and amounts of SFGs depending on the conditions and atmosphere. By choosing an appropriate activation method and condition,

*Corresponding author. Tel.: +81-87-869-3511; fax: +81-87-869-3550.

E-mail address: zm-wang@aist.go.jp (Z.-M. Wang).

0008-6223/02/$ – see front matter
PII: S0008-6223(01)00286-X

both structural and surface properties of ACs can then be tailored to the requirement of a particular application. Research regarding the design of the surface chemistry of ACs has been, up to now, limited to the surface modification of prepared ACs, which, sometimes, leads to a greater change in the pore structure [2]. With the aim of gaining a better understanding of the simultaneous controlling of pore structure and SFGs during preparation of ACs, the changes in porous structures and SFGs on activation and high-temperature treatment (HTT) of macadamia nutshell (MNS) char were studied in this research.

2. Experimental

2.1. Preparation and HTT of MNS-based ACs

The MNS-based ACs were prepared by the conventional two-step (carbonization–activation) method using a physical activation apparatus for which details are described elsewhere [19,20]. The preparation and treatment flow chart of the ACs are shown in Fig. 1. Australian MNS was mechanically crushed, milled, and sieved to obtain particles of around 1.2 mm in diameter. A 65-g aliquot of MNS particles was then subjected to carbonization in a quartz reactor (4.5 cm, I.D.) at 973 K for 2 h under a N_2 stream having a supplying pressure of 300 kPa and a continuous flow-rate of 150 STD ml/min. The produced char was transferred to another quartz reactor (4.5 cm, I.D.), where physical activation was carried out at 1073 K with a CO_2 stream at a flow-rate of 150 STD-ml/min for 4, 10, and 20 h, from which ACs with burn-offs of 15, 35, and 67% were obtained, respectively. AC samples were designated as AC*x*, where *x* stands for the burn-off. The AC35% sample was then further treated in a quartz reactor (4.5 cm, I.D.) in air at 573, 873, and 1173 K for 1 h or under an N_2 stream at 1073 K for 2 h which are denoted the AC35%–(*a*)ox or AC35%–(*a*)N_2 samples, respectively. Here (*a*) in the sample name stands for the treatment temperature. AC35%–1173ox sample was retreated under an N_2 stream at 873 K for 2 h to obtain the AC35%–1173ox–873N_2 sample. The oxygen contents in AC*x* were determined by a EMGA-2800-type oxygen analyzer (Horiba, Tokyo).

2.2. Determination of porosity

The porosity of the prepared ACs was determined by N_2 adsorption at 77 K with a commercial volumetric apparatus (Belsorp 18A, Bellsorp, Osaka), which can measure the amount of adsorption from 1.32×10^{-4} kPa with an accuracy of 0.25% of the reading pressure values. The adsorption amount in the low pressure range was calculated after correction for pressure due to the thermal transpiration effect by the Takaishi–Sensui equation

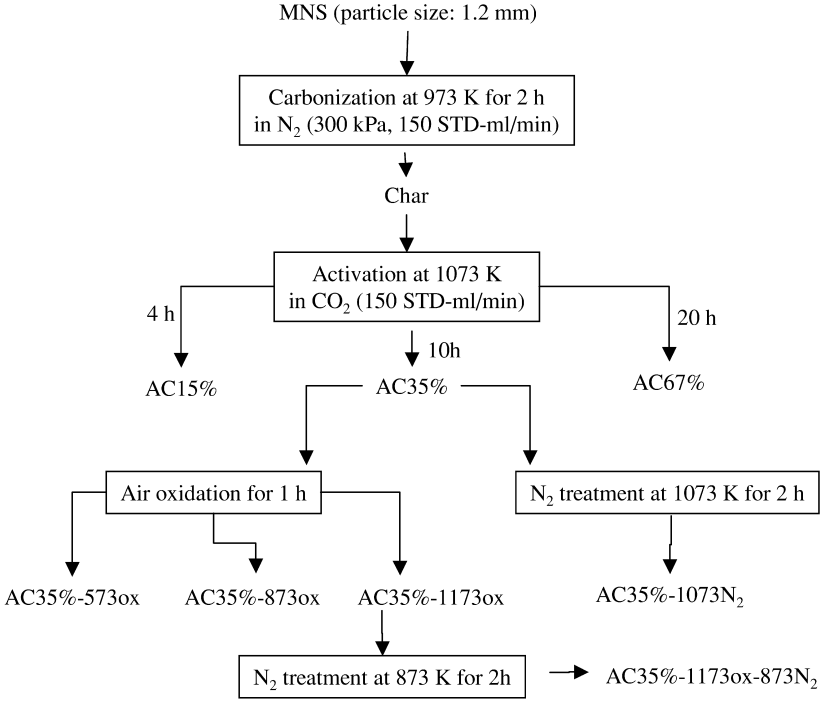

Fig. 1. Method of AC preparation and high temperature treatment.

[21,22]. The AC samples were pre-evacuated at 393 K below 1 mPa for 1 h prior to N_2 adsorption.

2.3. Determination of SFGs

The type of SFGs on ACs were studied by diffuse reflectance infra-red Fourier transform (DRIFT) spectrometer using a NEXUS 470-type FT-IR equipment (Nicolet, Tokyo) having a MCT ($Hg_{1-x}Cd_xTe$) detector. Samples without grinding and dilution with KBr and the background KBr were dried in air at 393 K for more than 3 days before being placed on the temperature-controllable sample holder in the DRIFT chamber. All the systems including the equipment accessories and the DRIFT chamber were purged by a continuous flow of N_2 gas of 99.999% purity during the measurements. After the samples were quickly transferred from the drier to the sample holder whose temperature was previously maintained at 393 K, the DRIFT spectra were monitored and were not recorded from 256 scans in a resolution of 2 cm^{-1} until the CO_2 species in air disappeared from the spectra. The spectrum of the pure KBr was used as the reference. The obtained DRIFT spectra were expressed by the Kubelka–Munk (K–M) function.

The C1s spectrum of the X-ray photoelectron spectroscopy (XPS) of ACs was measured under a vacuum of 10^{-6} Pa using MgK_α radiation (6 kV/30 mA) with a ESCA 850 apparatus (Shimadzu, Kyoto). AC samples without grinding were used for the measurements. The position of the binding energy was calibrated with respect to that of Au $4f_{7/2}$ (83.8 eV). The XPS spectra were curve-fitted by a non-linear least-square iterative technique based on the Gaussian function after baseline subtraction. The position of the most intense graphitic carbon peak was taken as 284.6 eV. The full width at half maximum of the deconvoluted peaks were 1.64±0.17 eV. The molecular contents of the SFGs were calculated from the ratio of peak area of the corresponding deconvoluted peak to that of the graphitic carbon.

Temperature-programmed desorption (TPD) of char and ACs was carried out in a He stream with a constant flow-rate of 20 STD ml/min at a ramp-rate of 10 K/min using an Okurariken TP-5000 apparatus. Outgases were analyzed by a Q-MASS spectrometer (ULVAC MMC-400, Yokohama). Prior to the TPD experiments, the samples were dehydrated at 393 K for 1 h under a He stream in the same quartz reactor used for TPD.

3. Results and discussion

3.1. Evolution of pore structure on activation and HTT

Fig. 2 shows the N_2 adsorption isotherms on the char and ACs at 77 K. All N_2 adsorption isotherms are of typical type I [1,3]. The char sample has the smallest N_2 adsorption amount. The N_2 adsorption amount on ACs monotonously increased with the increase of activation extent. HTT of AC35% in N_2 shows only a little effect on the increase in N_2 adsorption amount, whereas that in air at 1173 K brings about an enormous increase in N_2 adsorption. The N_2 adsorption isotherm of AC35%–1173ox has a gradual increase above $P/P_0=0.2$, indicating the presence of larger pores. No evident hysteresis is observed in the N_2 adsorption isotherms of the AC samples. However, an explicit hysteresis is observed for the char, indicating non-equilibration upon adsorption due to the small size of the micropores.

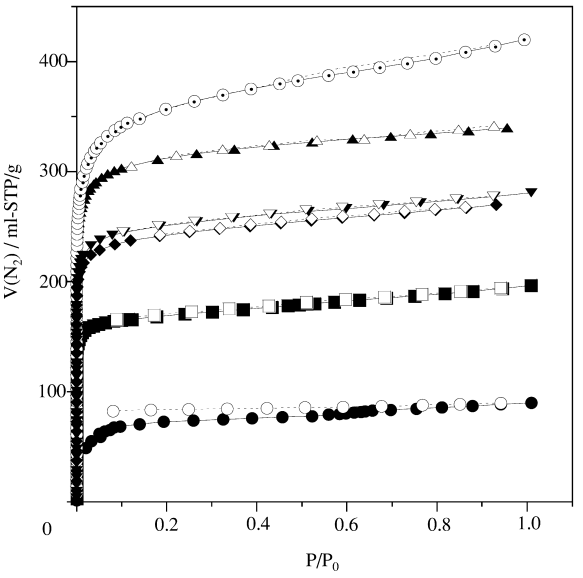

Fig. 2. N_2 adsorption isotherms at 77 K on the char (●, ○), AC15% (■, □), AC35% (♦, ◇), AC67% (▲, △), AC35%–1073N_2 (▼, ▽), and AC35%–1173ox (⊙, •). Open symbols represent desorption branches.

The following Dubinin–Radeshekevich (DR) equation was applied to the analysis of the N_2 adsorption isotherms [5,6]:

$$\ln W = \ln W_0 - (RT/\beta E_0)^2 \ln^2 (P_0/P) \quad (1)$$

where W and W_0 are the adsorption amounts at pressure P and the saturated vapor pressure P_0, respectively; β and E_0 are the affinity coefficient and characteristic adsorption energy of N_2, respectively; R is the universal gas constant; and T is the adsorption temperature. Fig. 3 shows the DR plots of char and ACs. All the DR plots can be divided into three regions: (1) a downward bending at the lowest pressure range [$P/P_0<10^{-4}$ or $\ln^2 (P_0/P)>85$], (2) a linear range at $10^{-4}<P/P_0<0.04\sim0.1$ [or $5.3\sim8<\ln^2 (P_0/P)<85$], and (3) a slight uprising at $P/P_0>0.1$ [or $\ln^2 (P_0/P)<5.3$]. Recently, Ohba et al. [23,24] showed that just the linear range (2) can provide information on a

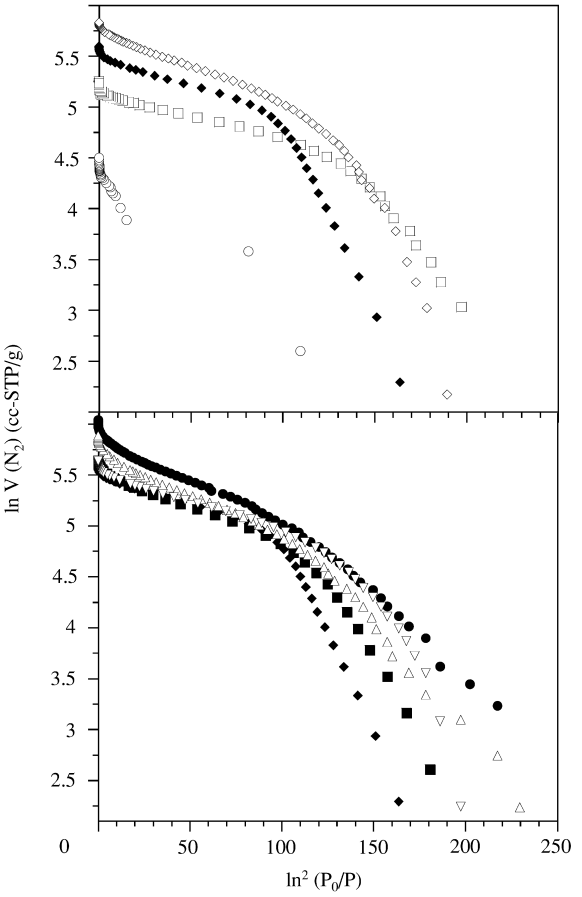

Fig. 3. DR plots of N_2 adsorption isotherms on the char (○), AC15% (□), AC35% (♦), AC67% (◇), AC35%–1073N_2 (▽), AC35%–873ox (■), AC35%–1173ox (●), AC35%–1173ox–873N_2 (△).

Gaussian type pore width distribution and the average pore width with the Dubinin–Stoeckli relation [25,26]. According to Marsh's classification on the type of DR plots [27], the downward bending range (1) can be ascribed to N_2 adsorption into the smallest micropores, i.e., the ultramicropores (UMP), while the uprising range (3) either to the cooperative micropore filling of N_2 in larger micropores (with a pore width larger than 0.7 nm) or to the multilayer condensation on the flat (external) surface. A complete equilibrium may not be obtained for N_2 adsorption in range (1) due to diffusion obstacles or another activation barrier. Although even adsorption in a uniform micropore gives the downward deviation of a DR plot in the lowest pressure range by the GCMC simulation [23], comparison of the N_2 adsorption amount in this range and the position crossing the linear range (2) can provide information on the evolution of UMP (the amount or pore width) during activation and HTT because of the same time allowed for the equilibrium in every run. The very initial activation with a burn-off of 15% produces the longest range (2) with the smallest slope of all the ACs and range (1) with a very high N_2 adsorption, indicating the production of comparatively uniform micropores having smaller dimensions. A higher extent of activation with a burn-off of 35% leads to the production of large amounts of micropores forming range (2) and having a larger micropore size [a greater slope of range (2)] but at the expense of the smallest micropores. The high activation extent giving a burn-off of 67% brings about the production of large amounts of micropores forming range (2), which have almost the same average pore size (the same slope) as that of AC35%. A higher N_2 adsorption in UMP is also brought about for AC67% on the consequence of both the pore opening of the previously formed UMP and the formation of the new UMP by adequate activation. On the other hand, HTT in N_2 and air treatment below 873 K mainly induces the development of UMP without any significant effect on the evolution of larger micropores, i.e., the supermicropores (SMP). However, air treatment at a high temperature (1173 K) increases both the SMP as well as UMP, which are almost uniformly reduced by further HTT in N_2. Table 1 shows the values of the micropore volume, $V_{0,DR}$, βE_0, and the adsorption energy at the fractional filling of $1/e$, $q_{st,1/e}$, by the following equation:

$$q_{st,1/e} = \beta E_0 + \Delta H_L \quad (2)$$

Table 1
Porosities of the char and ACs determined by DR- and α_s-plots

Sample	$V_{0,DR}$ (cc g^{-1})	βE_0 (kJ/mol)	$q_{st,1/e}$ (kJ/mol)	$V_{0,s}$ (cc g^{-1})	$A_{s,total}$ (m^2 g^{-1})	$A_{s,ext}$ (m^2 g^{-1})	w (nm)
Char	0.11	4.4	10.0	0.12	241	15	0.98
AC15%	0.26	10.3	15.9	0.26	750	20	0.72
AC35%	0.37	9.0	14.6	0.40	1047	16	0.77
AC67%	0.47	8.0	13.6	0.50	1336	20	0.76
AC35%–573ox	0.37	9.2	14.8	0.39	1079	12	0.74
AC35%–873ox	0.38	8.2	13.8	0.42	1101	12	0.77
AC35%–1173ox	0.51	7.5	13.1	0.58	1440	45	0.84
AC35%–1173ox–873N_2	0.44	7.5	13.1	0.49	1255	59	0.81
AC35%–873N_2	0.38	9.0	14.6	0.41	1107	16	0.75

where ΔH_L is the liquefaction enthalpy of N_2 ($\Delta H_L = 5.6$ kJ/mol at 77 K [28]). The $V_{0,DR}$ can be enhanced to be 0.51 ml/g (AC35%–1173ox) in contrast to 0.11 ml/g of the char by the appropriate method of activation and HTT. The gradual decrease in βE_0 or $q_{st,1/e}$ values demonstrates the gradual increase in the average pore size of the part of SMP forming range (2) with the increase in activation extent.

Fig. 4 shows the α_s-plots from N_2 adsorption isotherms on char and ACs. Here, the standard data on non-porous carbon reported by Rodriguez-Reinoso et al. [29] was used because of a similar surface property [3,30] despite the fact that the α_s-values at the lower pressure range are not available. The α_s-plots of all the samples showed a straight line passing through the origin except for some deviation in the case of char and AC15%. The deviation of char and AC15% may be related to their different surface properties from the standard non-porous carbon [30] or partially originated from the cooperative swing effect which occurs in micropores of $w > 1$ nm [16,31,32]. Table 1 also shows the values of the pore volume, $V_{0,s}$, and the total and external surface areas, $A_{s,total}$ and $A_{s,ext}$, respectively, from the α_s-plots. While $V_{0,s}$ and $V_{0,DR}$ agree very well with each other for char and the low extent activation carbon, the $V_{0,s}$ values are greater than $V_{0,DR}$ for the higher extent activation carbons and the ACs after HTT, indicating a greater production of larger micropores (or little mesopores) by these conditions. The average pore width, w, of char and ACs was then calculated by the following equation:

$$w = 2V_{0,s}/(A_{s,total} - A_{s,ext}) \times 1000 \quad (3)$$

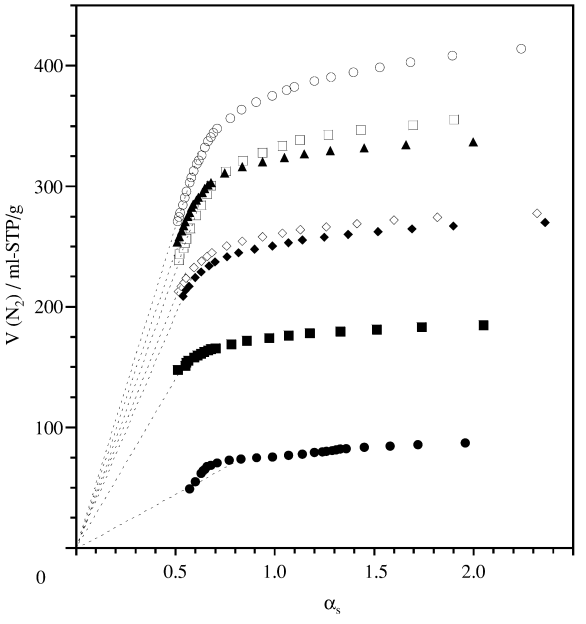

Fig. 4. α_s-Plots of N_2 adsorption isotherms on the char (●), AC15% (■), AC35% (♦), AC67% (▲), AC35%–1073N_2 (◇), AC35%–1173ox (○), and AC35%–1173ox–873N_2 (□).

where w can be a parameter reflecting the totally averaged porosities of char and ACs rather than only those of micropores forming range (2). As shown in Table 1, the char has the largest w values due to a greater fraction of large micropores. HTT of AC35% in air at 1173 K leads to the largest surface area due to the production of a larger fraction of larger micropores. Furthermore, a larger $A_{s,ext}$ value of AC35%–1173ox suggests the formation of larger macropores.

3.2. Evolution of surface functional groups on activation and HTT

Fig. 5 shows the DRIFT spectra of the char, AC15%, AC35%, AC67%, and AC35%–1173ox. The DRIFT spectrum of the char shows an obvious difference from the spectra of the ACs, having characteristic peaks at 1026 and 1609 cm^{-1} which can be ascribed to the ether bridge group possibly due to the lignocellulose texture and the C=C stretching mode of the exposed aromatic rings, respectively [17,33,34]. On the other hand, the DRIFT spectra of ACs show the appearance of new bands at around 1789, 1625, and 893 cm^{-1}, and the more evident peak at around 1320 cm^{-1}. The bands at 1789 and 1320 cm^{-1} can be ascribed to the lactone groups and those at 1625, 1320, and 893 cm^{-1} to the carbonate/carboxyl carbonate groups [33]. Another possibility that contributed to the growth of the 1625 cm^{-1} band is the formation of the –C=O group highly conjugated with the aromatic ring such as quinones. Zhuang et al. reported that this group grows with the increase of the gasification degree of a char [34]. All the carbon samples show a broad band at 3200–3500 cm^{-1}, indicating the presence of H-bonded H_2O [35] or the organic –OH groups, although the bands due to the organic –OH groups at around 1000–1300 cm^{-1} [33] are not detectable due to the overlapping of the strong 1320 and 893 cm^{-1} peaks. HTT of AC35% in air at 1173 K leads to the formation of more carbonate/carboxyl carbonate (1625, 1320, and 893 cm^{-1}) or quinone (1625 cm^{-1}) groups than lactone groups (1789 and 1320 cm^{-1}) in comparison with AC67%.

Fig. 6 shows the C1s XPS spectra of the char, AC15%, and AC67%, which are deconvoluted into four or five peaks after baseline subtraction using Shirleys' method [18,36–38]. Besides a symmetric peak centered at 284.6 eV due to graphitic carbon, four other deconvoluted peaks can be obtained for ACs, which are centered at 286.0, 287.3, 288.9, and 290.7 eV and assigned to –C–O bonding, –C=O or O–C–O bonding, O–C=O bonding, and carbonate species, respectively. However, a satisfactory result from curve-fitting cannot be obtained for the char unless unifying the two peaks at 286.0 and 287.3 eV into one centered at 286.7 eV. This unified peak at 286.7 eV can be considered as the overall contribution from the –C–O and –C=O bondings. Therefore, the different deconvolution results for char and ACs with respect to the peak positions

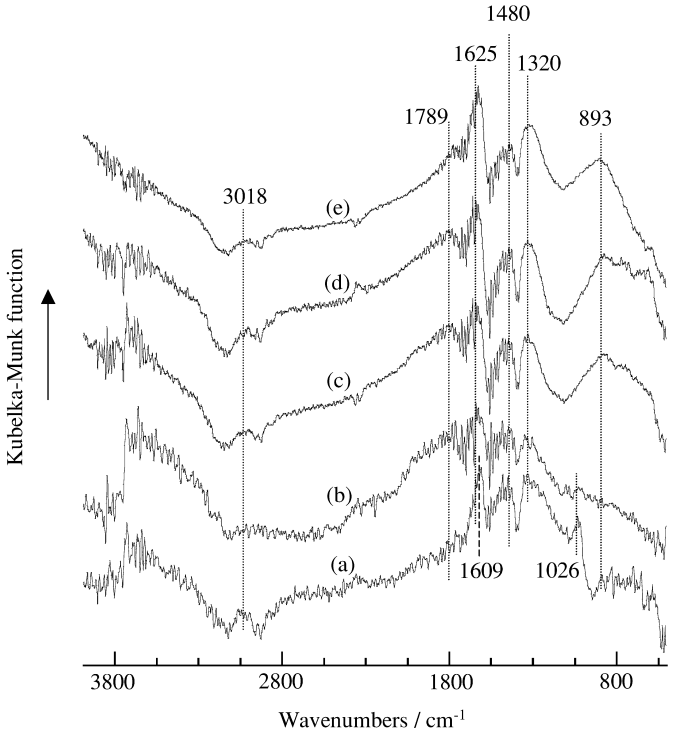

Fig. 5. DRIFT spectra of (a) the char, (b) AC15%, and (c) AC35%.

at 286–287.3 eV demonstrate that the –C–O and –C=O/O–C–O groups on char have different chemical environment in comparison with those on ACs. This corresponds to the results from the DRIFT measurements and will be further confirmed by the later TPD results. Table 2 shows the positions of the deconvoluted peaks, the molecular fractions of each SFG, and the molecular ratios of total SFGs (C_{ox}) to graphitic carbon (C_{gr}) for the char and ACs. Activation leads to the increase in the C_{ox}/C_{gr} value from 0.22 to 0.57, demonstrating that the amount of SFGs increases with the increase of activation extent. Elemental analysis results showed that the oxygen contents are 9.4 wt.% for the char, 9.7 wt.% for AC15%, 14.6 wt.% for AC35%, and 16.8 wt.% for AC67%. In spite of the similar oxygen content, AC15% presents more SFG amounts than the char, indicating that only one portion of oxygen-containing groups are exposed to the char surface that can be efficiently detected by the XPS method. Furthermore, increasing the activation extent (from 15 to 67%) preferentially increases the fraction of –C–O and –C=O groups, indicating that the higher extent activation is possibly controlled by the reaction between the carbon and the activating gas ($-C + CO_2 \rightarrow -C(O) + CO$).

Fig. 7 shows the TPD results of the char and ACs. Here the amount of the various evolved gases were compared by their relative intensities averaged by the sample weights rather than by the absolute quantities. There are evolutions of CO_2 and H_2O at around 600 K and CO, CO_2, H_2O, and H_2 at around 1000~1100 K for the char, whose positions are different from those for ACs, demonstrating their different types of oxygen-containing groups. All the ACs show the same peak positions for all the evolved gases, indicating that the types of their oxygen-containing groups are basically similar with each other as observed by the DRIFT spectra. Table 3 shows the total amount ratios of the evolved CO_x, CO_2, and H_2O from 373 to 1273 K from ACs with respect to those from the char. The very initial activation forming AC15% leads to an increase in the total amount of CO_x but a decrease in the amount of H_2O in comparison with the char. Since AC15% and the char have a similar oxygen content and the XPS results manifested that AC15% has more SFGs than the char has, the initial activation forming AC15% has relationship with the reactions involving the bulk phase oxygen-containing groups of the char which are not preferentially exposed to the surface. The production of SFG on AC15% may be considered as the overall results of the cracking and disappearing of the bulk phase oxygen-containing groups, and the new reactions involving the activating gas (CO_2). Hence, the very initial activation only leads to a change in the type and distribution of oxygen-containing groups but does not lead to a change in their amounts. On the other hand, higher extent activation gives a greater evolution of CO_x groups in correspondence with the higher amount of –C–O and –C=O groups from XPS results, again indicating that their forming process is mainly controlled by the

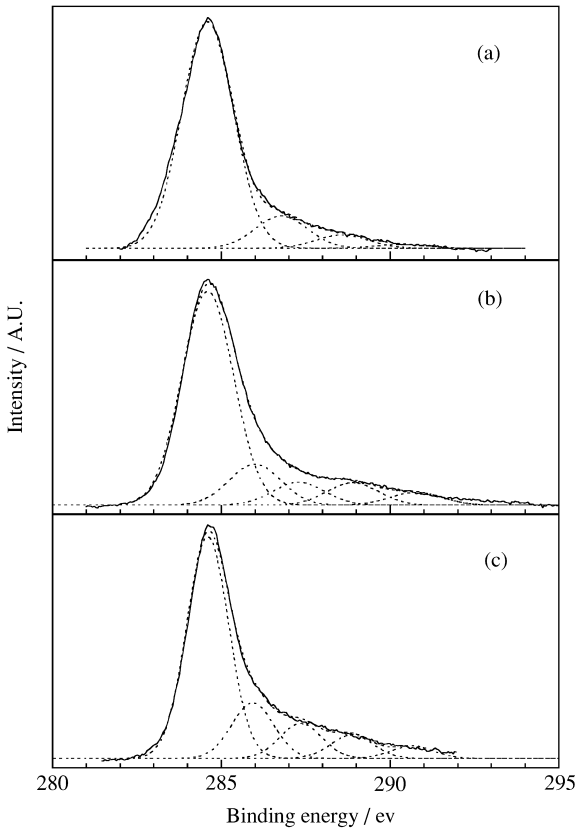

Fig. 6. C1s XPS peaks of the char and activated carbons.

reactions between carbon and the activating gas (CO_2). However, AC35% has a greater amount of the evolved H_2O than AC67%, suggesting that AC35% has a different profile in terms of the fraction of each SFG from that of AC67%. This may have relationship with its reduced UMP amount (Fig. 3) in comparison with AC15% as well as AC67%. Similar to the AC67%, HTT of AC35% in air at 1173 K leads to formation of greater amounts of –C–O and –C=O groups by the vigorous reaction between carbon and oxygen. HTT of AC–1173ox in N_2 at 873 K leads to a decrease in the amounts of CO_x and CO_2 by the same ratio (a factor of 0.7). Considering the corresponding decrease of the equal amount of N_2 adsorption in the UMP and SMP ranges by this treatment (Fig. 3), the SFGs to evolve CO_x may distribute through the UMP to the SMP in AC35%–1173ox, whose detachment induces a uniform diminishing of both UMP and SMP.

4. Conclusion

Macadamia nut-shell (MNS) char has one part of micropores of very small size, which leads to nonequilibration nitrogen adsorption. The initial activation forming AC15% produces comparatively uniform micropores having smaller dimensions and the developed ultramicropores (UMP). Increasing the activation extent increases both the micropore volume and the size of supermicropores (SMP). High temperature treatment (HTT) of AC35% in N_2 or in air at a lower temperature does not have a significant effect on the change of SMP, but gives rise to the development of UMP. HTT of AC35% at 1173 K greatly increases the micropore volume and the fraction of larger micropores.

The oxygen-containing groups of the MNS char mainly exist in its bulky phase with smaller amounts exposed to the surface. The SFGs of the char are different from those on ACs by DRIFT, XPS, and TPD results. The XPS and TPD results indicate that low extent activation of MNS char possibly has a relationship with the cracking and disappearing of the bulky phase oxygen-containing groups. Increasing the activation extent basically increases the content of SFG. High extent activation and HTT of AC35% in air at 1173 K preferentially increases the amount of –C–O and –C=O groups by vigorous reactions between carbon and the activating gas (CO_2 or O_2).

Acknowledgements

ZMW thanks the Department of Chemical Engineering of UQ for financial support of a short-period postdoctoral fellowship. Dr. P. Fredricks and Dr. Y. Nishi are gratefully acknowledged for their beneficial discussion and technical assistance in DRIFT and XPS measurements. Part of the

Table 2
Quantitative determination of SFGs on char, AC15%, and AC67% by XPS

Sample	Binding energy [eV (mol%)]					C_{ox}/C_{gr}
	C–C	C–O	C=O or O–C–O	O–C=O	$-CO_3$	
Char	284.6 (82.2)		286.7 (11.7)	288.6 (4.8)	290.3 (1.3)	0.22
AC15%	284.6 (68.4)	286.0 (13.1)	287.3 (7.3)	288.9 (7.1)	290.8 (4.1)	0.46
AC67%	284.6 (63.8)	285.9 (15.9%)	287.4 (10.0)	288.9 (6.7)	290.7 (3.5)	0.57

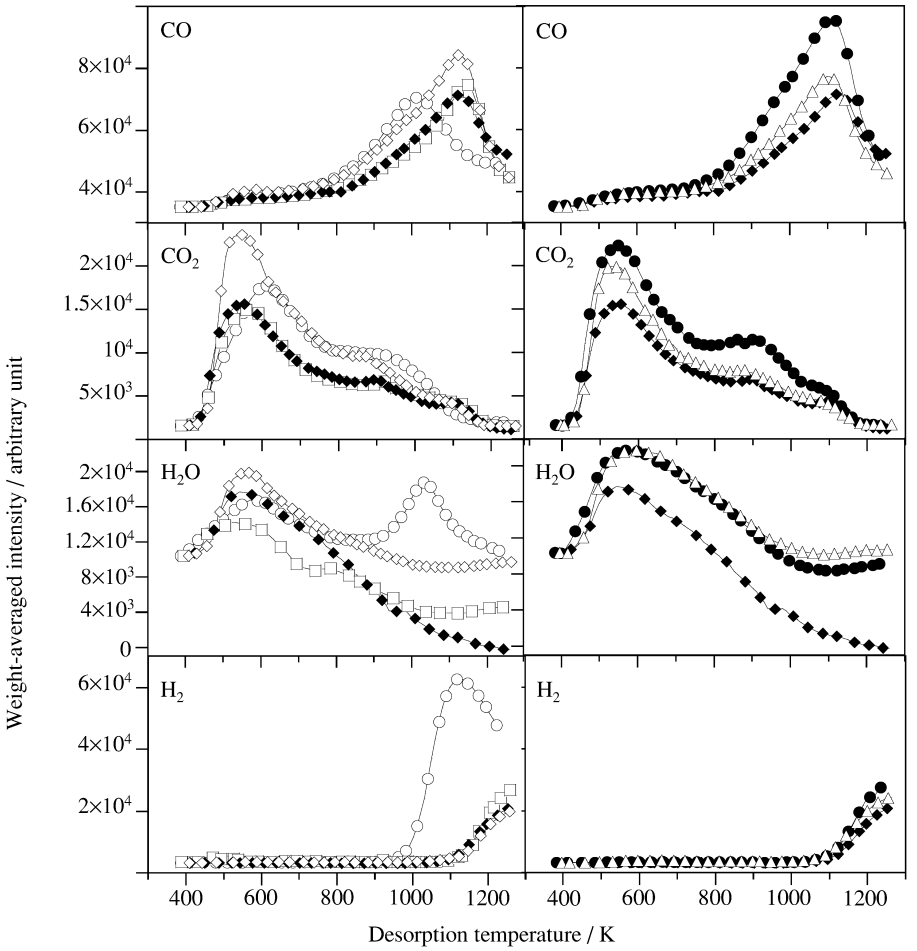

Fig. 7. TPD curves of the char (○), AC15% (□), AC35% (♦), AC67% (◇), AC35%–1173ox (●), and AC35%–1173ox–873N_2 (△).

Table 3
Total amount ratios of the evolved CO_x, CO_2, and H_2O from ACs with respect to those from the char

Sample	Total amount ratios		
	CO_x	CO_2	H_2O
AC15%	1.19	0.75	0.56
AC35%	1.26	0.80	1.11
AC67%	2.03	1.14	0.94
AC35%–1173ox	2.18	1.29	1.53
AC35%–1173ox–873N_2	1.54	0.92	1.38

AC samples was prepared with the help of Dr. A. Ahmadpour and Dr. C. Nguyen.

References

[1] Rouquerol F, Rouquerol J, Sing KSW. Adsorption by powders and porous solids. San Diego: Academic, 1999.
[2] Radovic LR, Rodriguez-Reinoso F. Chem Phys Carbon 1997;25:243.
[3] Gregg SJ, Sing KSW. Adsorption, surface area, and porosity. New York: Academic, 1982.
[4] Bond RL. Porous carbon solids. New York: Academic, 1967.
[5] Dubinin MM. Chem Rev 1960;60:235.
[6] Bering BP, Dubinin MM, Serpinsky VV. J Colloid Interface Sci 1966;21:378.
[7] Kaneko K. Langmuir 1987;3:357.
[8] Wang Z-M, Shindo N, Otake Y, Kaneko K. Carbon 1994;32:515.
[9] Boehm HP. Adv Catal 1966;16:198.
[10] Raymundo-Piñero E, Carzorla-Amorós D, Salinas-Martinez de Lecea C. Carbon 2000;38:335.
[11] Mochida I, Sakanishi K. Fuel 2000;79:221.
[12] Martinmartinez JM, Singoredjo L, Mittelmeijerhazeleger M, Kaptejin F, Moulijn JA. Carbon 1994;32:897.
[13] Marsh H, Crawford D, O'Grady TM, Wennerberg AN. Carbon 1982;20:419.
[14] Dai X, Antal Jr. MJ. Ind Eng Chem Res 1999;38:3386.
[15] Conesa JA, Sakurai M, Antal Jr. MJ. Carbon 2000;38:839.
[16] Kaneko K, Ishii C, Ruike M, Kuwabara H. Carbon 1992;30:1075.

[17] Zawadzki J. Chem Phys Carbon 1989;21:147.
[18] Brigg D, Seah MP. Practical surface analysis, 2nd ed.. New York: John Wiley and Sons, 1995.
[19] Nguyen C, Do DD. Carbon 1995;33:1717.
[20] Ahmadpour A, Do DD. Carbon 1996;34:471.
[21] Takaishi T, Sensui Y. Trans Faraday Soc 1963;59:2503.
[22] Poulter KF, Rodgers MJ, Nash PJ, Thompson TJ, Perkin MP. Vacuum 1983;33:311.
[23] Ohba T, Suzuki T, Kaneko K. Carbon 2000;38:1879.
[24] Ohba T, Suzuki T, Kaneko K. Chem Phys Lett 2000;326:158.
[25] Dubinin MM, Stoeckli HFJ. Colloid Interface Sci 1980;75:34.
[26] Dubinin MM. Carbon 1983;21:359.
[27] Marsh H. Carbon 1987;25:49.
[28] Lide DR, editor, Handbook of chemistry and physics, 76th ed., Boca Raton: CRC Press, 1995, pp. 6–117.
[29] Rodriguez-Reinoso F, Martin-Martinez JM, Prado-Burguete C, McEnaney BJ. Phys Chem 1987;91:515.
[30] Sing KSW, Everett DH, Haul RAW, Moscou L, Pierotti RA, Rouquerol J, Siemieniewska T. Pure Appl Chem 1985;57:603.
[31] Kaneko K, Ishii C, Kanoh H, Hanzawa Y, Setoyama N, Suzuki T. Adv Colloid Interface Sci 1998;76–77:295.
[32] Balbuena PB, Gubbins KE. Fluid Phase Equilib 1992;76:21.
[33] Fanning PE, Vannice MA. Carbon 1993;31:721.
[34] Zhuang Q-L, Kyotani T, Tomita A. Energy Fuels 1994;8:714.
[35] Fuller EL, Smyrl NR. Fuel 1985;64:1143.
[36] Kaneko Y, Ohbu K, Uekawa N, Fujie K, Kaneko K. Langmuir 1995;11:708.
[37] Kozlowski C, Sherwood PMA. Carbon 1986;24:357.
[38] Polovina M, Babic B, Kaluderovic B, Dekanski A. Carbon 1997;35:1047.